Talanta 102 (2012) 44–52

Contents lists available at SciVerse ScienceDirect

Talanta

journal homepage: www.elsevier.com/locate/talanta

Characterization of a constant current charge detector

Masanobu Mori [1], Yongjing Chen [2], Shin-Ichi Ohira [3], Purnendu K. Dasgupta *

Department of Chemistry and Biochemistry, The University of Texas at Arlington, Arlington, TX 76019-0065, USA

ARTICLE INFO

Available online 21 August 2012

Keywords:
Constant current charge detector
Electric field induced dissociation
Membrane electro-transport

ABSTRACT

Ion exchangers are ionic equivalents of doped semiconductors, where cations and anions are equivalents of holes and electrons as charge carriers in solid state semiconductors. We have previously demonstrated an ion exchange membrane (IEM) based electrolyte generator which behaves similar to a light-emitting diode and a charge detector (ChD) which behaves analogous to a p–i–n photodiode. The previous work on the charge detector, operated at a constant voltage, established its unique ability to respond to the charge represented by the analyte ions regardless of their redox properties, rather than to their conductivities. It also suggested that electric field induced dissociation (EFID) of water occurs at one or both ion exchange membranes. A logical extension is to study the behavior of the same device, operated in a constant current mode (ChD_i). The evidence indicates that in the present operational mode the device also responds to the charge represented by the analytes and not their conductivity. Injection of a base into a charge detector operated in the constant voltage mode was not previously examined; in the constant current mode, base injection appears to inhibit EFID. The effects of applied current, analyte residence time and outer channel fluid composition were individually examined; analyte ions of different mobilities as well as affinities for the respective IEMs were used. While the exact behavior is somewhat dependent on the applied current, strong electrolytes, both acids and salts, respond the highest and in a near-uniform fashion, weak acids and their salts respond in an intermediate fashion and bases produce the lowest responses. A fundamentally asymmetric behavior is observed. Injected bases but not injected acids produce a poor response; the effects of incorporating a strong base as the electrolyte in the anion exchange membrane (AEM) compartment is far greater than incorporating an acid in the cation exchange membrane (CEM) compartment. These observations suggest that EFID occurs primarily at the anion exchange membrane and is inhibited by the presence of OH^-. Analyte peak widths and peak asymmetries were found to be governed by the mobility of the analyte ions and their affinities for the IEMs, respectively.

1. Introduction

Almost half a century ago Maslov and Zolotov wrote a provocative review titled *Water as a semiconductor* [1]. At 25° C, intrinsic charge carrier pair densities in Ge, Si and GaAs are, respectively, 2×10^{13}, 9×10^{9}, and 2×10^{7} cm^{-3} [2], while that for water is 6×10^{13} cm^{-3}. The mobilities in the different matrices are very different, however, resulting in respective electrical resistivities of 60, 2×10^{5}, 1×10^{8}, and 2×10^{7} Ω cm. With anions and cations rather than electrons and holes as charge carriers, ion exchangers are the ionic equivalent of doped semiconductors. This paper exploits the behavior of ion exchange membranes (IEMs) as semiconductor devices in solution. This paper is dedicated as a tribute to Academician Yurii Aleksandrovich Zolotov on the occasion of his 80th birthday and his far-reaching foresight.

1.1. Diode behavior of IEMs

Rectification of alternating currents were reported for biological membranes early [3]; Lovreček et al. first demonstrated this diode behavior for a solution of a polymeric acid (polymeric anion) and a polymeric base (polymeric cation) separated by a thin dialysis membrane [4]. Frilette [5] described the first practical bipolar ion-exchange membranes (BIMs) where one face is a cation exchange membrane (CEM) and the other face is an anion exchange membrane (AEM). He also observed that under reverse bias conditions (CEM side negative, AEM side positive), the diode breaks down above a certain applied potential. He first

* Corresponding author.
E-mail address: dasgupta@uta.edu (P.K. Dasgupta).
[1] Department of Chemistry and Chemical Biology, Graduate School of Engineering, Gunma University, Kiryu 376-8515, Japan.
[2] ThermoFisher Corporation, 1214 Oakmead Parkway, Sunnyvale, CA 94085, USA.
[3] Department of Chemistry, Kumamoto University, 2-39-1 Kurokami, Kumamoto 860-8555, Japan.

0039-9140/$ - see front matter © 2012 Elsevier B.V. All rights reserved.
http://dx.doi.org/10.1016/j.talanta.2012.07.058

postulated that enhanced water dissociation occurs in the interface. Senō and Yamabe subsequently reported more complete electrical characterization of such BIMs [6].

1.2. Water splitting in a bipolar membrane and the Onsager model

This electric field induced dissociation (EFID) of water, also called water splitting, and specifically its occurrence in a BIM under reverse bias have been investigated extensively. It has been widely used in the industry to convert aqueous salt solutions into acids and bases without chemical addition or electrolytic gas generation [7–9]. For these applications, the membrane is operated in the reverse biased mode. The breakdown is akin to that of a conventional solid state Zener diode [10], except that the i–V curve under reverse bias conditions is far less steep for the membrane diode. The occurrence of EFID under these conditions has been extensively discussed in the BIM literature [11–17]. At typical applied reverse voltages, the dissociation rate of water in BIMs is estimated to be 10^6–10^7 times faster than in free solution. The enhanced dissociation of weak electrolytes at high electric field was first observed by Wien [18] and is often called the "second Wien effect". It was subsequently studied experimentally in more detail by Schiele [19,20]. This effect has been invoked to explain EFID. Onsager laid out the path to perform coulombic calculations that in principle enables one to quantitatively estimate how much the dissociation rate will increase at a given field strength [21]. He showed that coulombic interactions arising out of an electric field will affect the rate of dissociation of an ion-pair but will not affect the recombination rate, thereby increasing the dissociation constant.

1.3. Quantitative issues with the Onsager equation

The problem with utilizing the Onsager equation quantitatively in the BIM case is that while the applied voltage may be accurately known, the field at the interface of a BIM is not. The interfacial water layer in a BIM, across which the voltage drop primarily occurs, is largely a hypothetical construct; its thickness is not accurately known. Essentially any value of the field strength can be conjured by assuming a convenient thickness for the water layer. Nevertheless, field strengths calculated based on best estimates of the water layer thickness and application of the Onsager equation result in dissociation rates at least three orders of magnitude smaller than the observed values [22]. Experimentally, since the original works of Wien [18] and Schiele [19,20], very little further work has been done (for a review until 1939, see [23]). The most recent studies are now 60 years old [24,25]. The Onsager model invokes that the ratio of the dissociation constant K_E observed under a field strength of E electron volts per meter to the dissociation constant K_0 observed at zero applied field is solely a function of the parameter b, where b is given by $\sim 0.1E/DT^2$ (D and T being the solvent dielectric constant and the absolute temperature, respectively) for a uni-univalent electrolyte. Further, b is independent of the absolute value of the dissociation constant or the concentration. In reality, at the same applied field, the EFID increases significantly as K_0 decreases [19,23]. In aqueous solution, the dissociation of electrolytes weaker than carboxylic acids have never been studied, much less electrolytes (if we should even referred to water as such) as poorly dissociated as water.

1.4. Does the applied field polarize covalent molecules?

Onsager himself left an escape door out of this dilemma. Consider that we can imagine water in three forms: (a) as the covalent molecule HOH, (b) as the ion pair H^+OH^- (where sufficient charge separation has occurred), and (c) as the fully dissociated ions H^+ and OH^-. Onsager painstakingly pointed out that his model only applies to the transition from (b) to (c). It is possible that the applied field also polarizes the molecules such that more ion-pairs are formed from the covalently bonded moiety. It is possible that the weaker the electrolyte, greater is this field-induced conversion. If the majority of water is present as covalently bonded HOH and more of the ion pair is formed from it under the influence of the field (whether or not this is catalyzed by weak-base anion exchangers [22]), the dissociation rate at any given electric field strength will be greater than that predicted by the Onsager equation. Unfortunately, there is no simple way to quantitatively assess the extent of conversion of the covalently bonded form to the ion pair and how this would vary from one type of molecule to another.

1.5. From the BIM to a membrane based electrolyte generator: similarity to a light-emitting diode

The junction in a BIM is not accessible either fluidically or electrically. If this was the case for a semiconductor, only simple electrical p–n diodes will be possible (note that in light emitting diodes (LEDs) and photodiodes (PDs), the junction is photonically accessible). Recently we conceived of an arrangement where a cation exchange resin bead and an anion exchange resin bead were deliberately separated by a macroscopic distance ($>100\ \mu m$) [26]. The exterior of each bead as well the space in between were fluidically accessible. Structurally it is similar to a p–i–n diode where water flowing between the beads serves the role of the insulator. In the forward biased mode (CEM side positive, AEM side negative), a cation can be injected from the CEM feed, and an anion from the AEM feed, permitting generation of different electrolytes (acid, base or salt) in the central channel [27], much like current controlled generation of photons from hole–electron recombination in an LED. However, because of the diversity of charge carriers in solution, one can generate many different electrolytes, unlike the case of a given LED where only one color of light can be generated. Nevertheless, the number of equivalents of the electrolyte produced (and thus at constant flow rate, the concentration) is linearly related to the current, much like an LED where the emitted light intensity is linearly related to the current.

1.6. The reverse-biased membrane-based p–i–n diode detects ions: a charge detector

The three fluid channels devices with were made with planar membranes as well, the AEM and CEM being 250 μm apart [28]. With pure water on all three channels (exterior to the CEM, exterior to the AEM and in between the two) of the device, current–voltage curves showed diode behavior in the positive direction. In the reverse direction, past a modest reverse voltage (extrapolated $V_{threshold} \sim 1.5$ V) [28], current conduction begins again. Although the slope of the i–V curve is much less in the reverse direction than under forward bias, this clearly suggests that the onset of enhanced ionization of water is occurring at a field strength of ~ 6 kV/m, whereas the Onsager model predicts that a field of 7200 kV/m is needed to induce a 5% increase in the dissociation rate.

Perhaps more importantly, in the reverse biased mode, the above CEM–AEM devices behave as the ionic equivalent of reverse biased p–i–n photodiodes. In a reverse-biased photodiode, photons of sufficient energy falling on the device generate hole–electron pairs, which then run respectively to the negative electrodes on the p-side and the positive electrode on the n-side, generating a current pulse. In much the same fashion, if an electrolyte, e.g., NaCl, is injected into a water carrier stream flowing between the two membranes, Na^+ proceeds through

the CEM to the negative electrode and Cl^- proceeds through the AEM to the positive electrode, generating a current pulse proportional to the charge carried by the transported ions. The device thus behaves not as a conductivity detector (CD), the mainstay of ion chromatography (IC) since the celebrated introduction of suppressed conductometric IC by Small et al. [29], but as a charge detector (ChD). A commercial version of the ChD has recently been introduced for capillary scale IC [30].

1.7. The charge detector vs. the conductivity detector

Despite its universal response to ions, conductometry is mobility-based; different electrolytes have vastly different specific conductance. In IC the response for each ion must thus be individually calibrated for. There are occasions where analytes are not available in pure form or are unstable, or when accurate standards are difficult to make because of hygroscopicity; this makes accurate quantitation difficult. In principle, the charge detector provides a coulometric measurement, provided that all the analyte ions are quantitatively transported. Conventional coulometry provides a sensitive means of for analytes that undergoes well-defined redox processes at accessible potentials [31,32] but remains inapplicable for the majority of ionic analytes, e.g., Na^+ or SO_4^{2-}, whose redox potentials lie beyond the solvent breakdown potentials or, e.g., with Cl^-, where the oxidation competes with water breakdown and is faradaically inefficient. A detector that would respond to all ions based on their charge is attractive; it obviates the need for standards, at least for strong electrolytes.

1.8. Superfaradaic behavior of a charge detector

We have demonstrated the three-channel ChD fabricated in both ion-exchange bead (IEB) and IEM forms [28], where a flowing stream of water was bounded by two closely-spaced oppositely-charged IEBs or IEMs, with flowing liquid on their anterior sides. A voltage was applied between the two Pt electrodes disposed in the liquid on the anterior sides with the cation exchanger side held negative relative to the anion exchanger side. The resulting current was measured. It was reasoned that the background current results from the transport of H^+ and OH^-, generated from the ionization of water, respectively through the CEM and AEM to the negative and positive electrodes. However, the magnitude of this current was greater than what would correspond to the known ion concentrations in pure water. This behavior can be rationalized with the view that as H^+ and OH^- are removed, the ionization of water continues to produce these ions. In fact, this is an interesting feature of the ChD, it produces relatively greater signals for a weak electrolyte compared to a CD. Detection by a CD does not perturb the dissociation equilibrium; in contrast, the ChD is fundamentally a deionizer [33]; further ionization is promoted by the demands of maintaining an equilibrium. Nevertheless, this background current was observed to undergo a sudden increase after the applied voltage was increased beyond a threshold value, which was actually below the threshold voltage needed to cause electrolysis (see the inset of Fig. 3 in Ref. [28]; it is reproduced here as Fig. S1 in the supporting information (SI) for convenience). When an ionic solute is injected into the central flowstream, the cations/anions migrate through the CEM/AEM to the negative/positive electrodes respectively, producing a pulse of current above the background. After integration to coulombs, the peak area was related to the charge carried by the ionic solutes. Depending on the applied voltage, the current peak area (hereinafter called the measured charge signal, Q_m) could be less or more than the charge Q_i represented by the electrolyte aliquot injected. Situations where Q_m is less than Q_i could be easily rationalized: this will occur when ions are transported subquantitatively to/through the IEMs. However, it is less straightforward to rationalize values of $Q_m > Q_i$; this was generally the case at higher applied voltages. We reason that EFID of water occurs in these devices at one or both membrane surfaces, rather than in the bulk water separating the membranes. It has been demonstrated that EFID can occur at either the CEM or the AEM, but is more pronounced at the latter [34]. The scenario that we envision is that under background conditions, much of the voltage drop occurs across the insulating water layer between the membranes and not across the membranes themselves. Depending on the absolute value of the applied voltage, EFID of water may or may not occur under background conditions. When an electrolyte is injected in the central channel, however, the voltage distribution changes: as the central channel becomes more conductive, less voltage is dropped across the central region and more voltage appears across the membranes. As a result, EFID either begins at the membrane surfaces, or if already present, it is enhanced. This additional ionization of water causes Q_m to exceed Q_i and hence a superfaradaic response is produced.

Thus, unless the applied voltage can be deliberately chosen to be in an optimum range (under which conditions it is possible for Q_m to exactly equal Q_i over at least a 10-fold concentration range, whence at least for strong electrolytes, equivalent ionic solutes generate essentially identical coulomb signals), the device may not behave as an absolute coulometer. The superfaradaic response is enhanced if conductive electrolyte solutions, rather than water, are used in the electrode channels as voltage drop in these regions is minimized.

1.9. A constant current charge detector (ChD_i)

To summarize, as described until now, a p–i–n diode like ion-exchange membrane device with three fluid channels and with water flowing through the central channel behaves as a "charge detector" when a constant reverse bias of appropriate magnitude is applied across the device and an electrolyte is injected into the central channel. However, under a variety of conditions, the response of this device can be superfaradaic. In this paper, we examine an alternative means of ion detection based on the same device configuration. In this case, instead of having a constant voltage applied across the electrode, a constant current is applied across them. As an electrolyte is introduced into the system, the voltage necessary to maintain the same current decreases and it is the voltage applied across the electrodes that is the measurand. Obviously, such an arrangement minimizes the influence of any EFID that may be occurring. Admittedly, naming such a device as a "charge detector" would be a misnomer; neither charge, nor current is measured in such an arrangement. It is only the identical physical configuration that leads us to keep the same general designation. It may also seem that the device is merely a different form of a conductivity detector; it may simply be measuring the change in voltage drop as the conductivity of the central channel increases. This paper will be the first attempt to characterize the response behavior of a charge detector operated under constant current conditions (hereinafter called ChD_i) and how different operational parameters affect its response behavior.

2. Experimental

2.1. Reagents

All chemicals used were reagent grade; solutions were prepared with 18.2 MΩ cm Milli-Q deionized water.

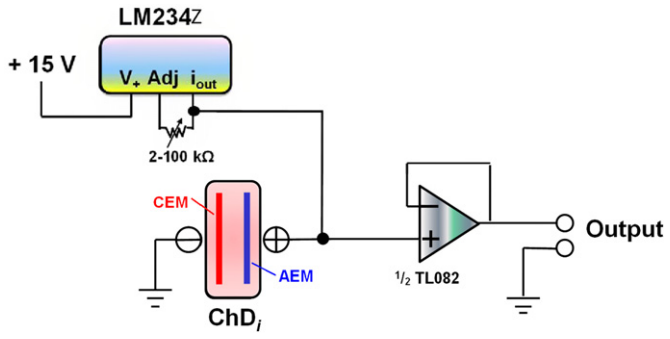

Fig. 1. The circuit arrangement of ChD operated at constant current (ChD_i).

2.2. Instruments

A ChD in the "membrane with screen-separated electrode (MSSE)" configuration was used for all experiments; see [28] for device construction. The device is based on Dionex 2 mm suppressor hardware and has the same active membrane area as a commercial suppressor; radiation-grafted poly(tetrafluoroethylene)-based ion-exchange membranes, custom-made by ThermoFisher/Dionex were used. The CEM and AEM are separated by a neutral screen whereas there are ion-exchange screens, correspondingly functionalized, adjacent to each of the membranes on the exterior side. Upon each functionalized screen, a platinized titanium screen electrode was placed. The three channels are fluidically isolated and independent flows can be established through each channel.

Water was delivered by a GP40 pump (Dionex) at 0.2 mL/min through the central channel; water or dilute electrolyte was delivered by gas pressure at 1.5 mL/min through the two other channels. Injection volume was 26.4 μL. A home-made constant current source based on a simple one-chip LM234z (⟨www.ti.com⟩) circuit was used; the device connections were not shielded. No efforts were made to thermostat the device; it was operated at the ambient laboratory temperature (~22° C). An unity gain voltage follower based on a FET input operational amplifier chip (TL082, www.ti.com) was used prior to connection to a Chromeleon™ data system (⟨www.dionex.com⟩) at 5 Hz through a UI20 interface system (⟨www.dionex.com⟩). The arrangement is schematically shown in Fig. 1. In this initial exposition, we focus on characterizing parametric effects on device behavior rather than attaining the best possible limits of detection (LOD).

Conductivity detectors (Dionex CD25, Dionex CDM-II) were used to monitor the change in conductivity of central channel before and after the ChD_i.

3. Results and discussion

3.1. Constant current mode vs. constant voltage mode

Both constant voltage and constant current devices are operated in the reversed bias mode. The signal to noise ratio (S/N) was tested with water flowing through all three channels and injecting 50 μM (1.32 nmol) KNO_3. The results are shown in Fig. S2 in the Supporting Information (SI). For the constant voltage mode, the occurrence of the maximum was pronounced at an applied voltage of 2 V. In the constant current case, the best S/N was observed at $i_{app}=1$ μA and it was a factor of ~3.5 × higher than in the constant voltage mode. (It should be noted that the comparison is based on the same device. The constant voltage mode produces much better S/N with smaller membrane area devices.)

For the ChD_i, over the entire range of 2–20 μA, a nearly constant 80–85% of this maximum S/N observed at $i_{app}=1$ μA was maintained; in the constant voltage mode, the drop-off in S/N from the optimum was much more pronounced.

Prima facie, if we consider the ChD_i as a device akin to a conductivity detector, i.e, simply operating as a resistive element, the voltage applied to attain some constant current will decrease as an analyte is injected into the central channel causing the central channel electrical resistance to decrease. Qualitatively this general behavior is observed. However while the effect, decrease in the applied voltage to maintain a constant current, is the same, the cause can either be due to increased conductivity or due to an increase in the total amount of charge per unit volume. The two are subtly different: isoconductive solutions do not necessarily have the same amount of charge per unit volume. This will be explored in Section 3.2.

Presently, it is of interest to note that even with zero voltage applied in the constant voltage mode or zero current forced in the constant current mode, significant current/voltage signals with good (but not the best) S/N is seen (Fig. S2). However, these seemingly simplest operational modes without applied potential are not attractive in practice because there is no significant motive force to remove the ions from the membranes and the response gradually decreased with the passage of time.

3.2. Does EFID occur? Does the device respond to conductivity or charge content?

Fig. S3 shows the voltage necessary to maintain fixed levels of current. Other than the datum for zero current, the rest of the data essentially shows a linear relationship with a *Y*-intercept of 0.74 V. For a membrane separation of ~250 μm [28] and an estimated electrode separation of ~500 μm for 75 μm thick membranes, a threshold voltage of 1.5 kV/m can be calculated for the onset of EFID. It would also appear that this threshold voltage drops entirely across the membrane and it is the additional potential above this drop that then linearly governs the current. The dynamic resistance of the device is calculated to be 88.3 kΩ from the slope. The active area of the central channel is 3.64 cm^2, for an electrode separation of 0.05 cm, one would calculate a specific resistance of 6.4 MΩ cm. This connotes an 8-fold increase of the water dissociation constant to $\sim 8\times10^{-14}$. This is modest and does not necessarily provide evidence for the occurrence of EFID, as even a small extent of impurity can cause this extent of conductivity increase. The existence of a threshold voltage for current conduction can then be explained by a threshold voltage needed for ion movement through ion exchange membranes, although the existence of such a threshold has never been established.

Regardless of the occurrence of EFID, whether the device really responds to conductivity or to charge under the constant current operation mode is of interest. We injected the same number of equivalents (1.32 neq) of three different strong electrolytes in 50 μM concentration: $NaClO_4$, $NaNO_3$ and HNO_3; the respective ratio of equivalent conductance values are 1:1.03:3.57. The results in Fig. 2 show that regardless of the value of i_{app}, equivalent amounts of strong electrolytes carrying equivalent charge generate signals of equivalent magnitude. It is to be noted that these electrolytes vary significantly either in their conductance or the affinity of at least one component ion for the corresponding IEM: Na^+ has considerable greater affinity for the sulfonic acid type CEM than H^+, similarly ClO_4^- has much greater affinity for the AEM than NO_3^-. The results leave little doubt that the device is responding to the charge present in the solution and not to its conductivity.

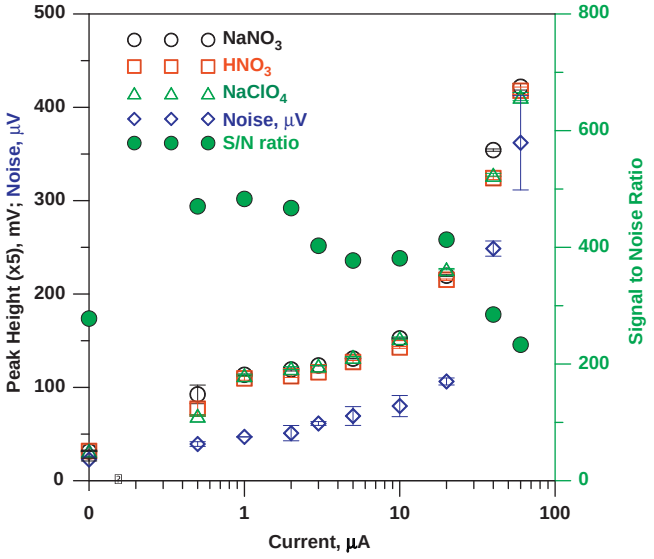

Fig. 2. Peak height and noise as a function of applied current. Central channel: water at 0.2 mL/min; outer channels: water at 1.5 mL/min; injected sample: 1.32 nmol of $NaNO_3$, $NaClO_4$, HNO_3 (50 μM concentration). The abscissa is in log scale for clearer depiction of low current data but the axis is interrupted before the origin to show the zero current results. The S/N values are shown only for $NaNO_3$ for clarity; the data for the other two analytes are very similar.

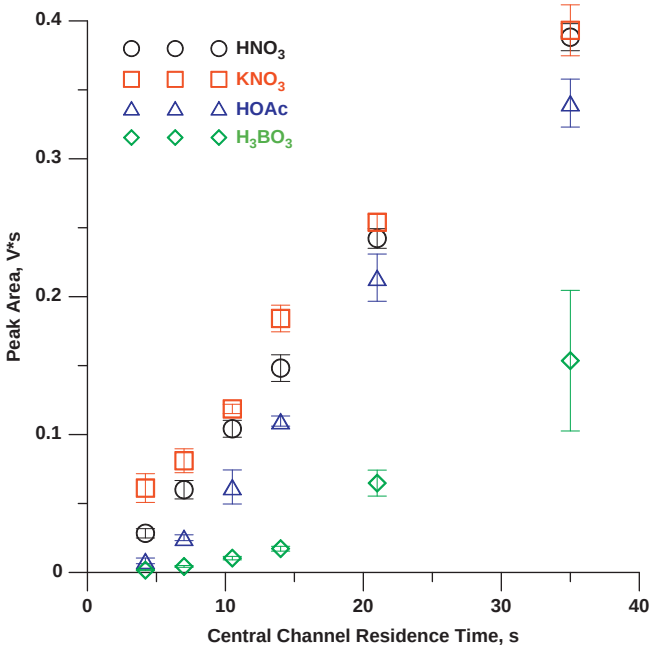

Fig. 3. Peak area as a function of central channel flow rate. Applied current, 25 μA; central channel: water at 0.06–0.5 mL/min; outer channels: 1 mM HNO_3/1 mM KOH at 1.5 mL/min; injected sample: 50 μM of HNO_3, KNO_3, HOAc, H_3BO_3; injected volume: 26.4 μL.

The signal and noise both increase monotonically with increasing i_{app} but the rates of increase of both are comparable in the i_{app} = 0.5–20 μA range. Although there is a maximum in S/N at i_{app} = 1 μA, the S/N values throughout this i_{app} range is comparable, as previously seen in Fig. 2. However, a steep increase in the signal and even more so in the noise takes place at $i \geq 20$ μA, resulting in a decrease in S/N above this i_{app}. The transition takes place somewhere between i = 10–20 μA, corresponding to V_{app} = 1.6–2.5 V, when electrolysis observably begins.

3.3. *Effect of analyte residence time in detector*

The residence time and the current level will both govern how much of the injected analyte will be transferred through the membranes. This was examined at a fixed current level of 25 μA for residence times of 4.2–35 s (flow rates of 60–500 μL/min) while injecting 1.32 neq of HNO_3, KNO_3, HOAc, and $B(OH)_3$, respectively. As a reference point, 25 μA flowing for 10 s is faradaically equivalent to 2.6 neq. The extents of removal, calculated from conductivity detector peaks before and after the ChD_i, are shown in Fig. S4 in the SI. These data indicate that the maximum removal (attained with HNO_3 with $t_R \geq 20$ s) is ca. 75%. The extent of removal appears to be a function of both dissociated ion concentrations and their mobilities. The fact that the analyte does not account for the total coulombs passed during its passage indicates that as under background conditions, some of the transported charge comes from H^+ and OH^- generated by the dissociation of water. For constant voltage mode ChD operation, it was observed that the behavior of a weak electrolyte compared to that of a strong electrolyte is markedly different as a function of the central channel flow rate. The peak area for a weak electrolyte (in coulombs) increases notably at increased values of detector residence time. It was reasoned [28] that as some of the dissociated weak electrolytes are removed through the membranes, more is ionized and further removal is aided by additional residence time. However, there is also another possibility. During the entire time, the analyte peak appears, EFID, above and beyond background conditions, contributes to the observed peak area. Prolonging the time over which the peak appears increases this contribution proportionately. An increase in the peak area with increased residence time is thus also observed for a strong electrolyte but to a smaller extent in relative terms. The latter will be expected: if we encounter the same absolute contribution of EFID to the peak area from both the strong and weak electrolyte cases, the contribution of the dissociated analyte itself to the observed peak area in the strong electrolyte case is much larger; the EFID contribution will therefore be smaller. In the present case, as shown in Fig. 3, peak areas for HNO_3, KNO_3, and HOAc all increase essentially linearly with increasing detector residence times with nearly the same slope. In contrast, boric acid shows a different behavior; at high residence times, the peak area increases exponentially with the residence time. At least in the case of this very weak acid, these data suggest some step(s) other than the transport of the already ionized analyte species and linear summation of water–EFID derived H^+ and OH^- are involved. Because boric acid ionization actually involves the reaction of $B(OH)_3$ with OH^- and from a forward rate constant of the reaction $B(OH)_3 + OH^- \rightarrow B(OH)_4^-$ of $10^7\ M^{-1}\ s^{-1}$ [35] at a pH of 6 will lead to a half-life for ionization of 7 s, and the generated $B(OH)_4^-$ ion will then have to be transported to the electrodes. This is not inconsistent with the timescale of the observed behavior of $B(OH)_3$.

3.4. *Outer channel fluid composition*

As a forethought, we assumed that the solution composition of the outer channels will affect the voltage drop in the electrode compartments and possibly that of the membrane as well, thus affecting the total voltage across the device for the same i_{app}. This in turn should affect the signal, noise and S/N. While the electrode compartment solution composition certainly affected the performance parameters, the presumption that electrode solution conductivity will be the causative parameter proved to be incorrect. In the following, the solution composition is cited in the CEM/AEM order, i.e., w/w connotes there is water on both the CEM and AEM channels, while a/b connotes that there is acid (1 mM HNO_3)

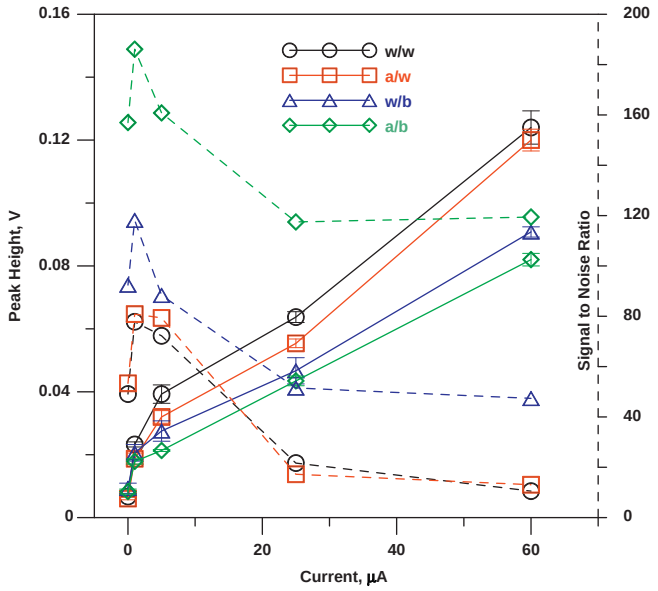

Fig. 4. Peak height (solid lines) and signal to noise ratio (dashed lines) as a function of current with different electrolyte compositions in the outer channels. Central channel: water at 0.2 mL/min; outer channels (CEM/AEM) composition: water/water (w/w), 1 mM HNO_3/water (a/w), water/1 mM KOH (w/b), 1 mM HNO_3/1 mM KOH (a/b). Outer channel flows are 1.5 mL/min respectively; injected sample: 50 μM KNO_3, 1.32 nmol.

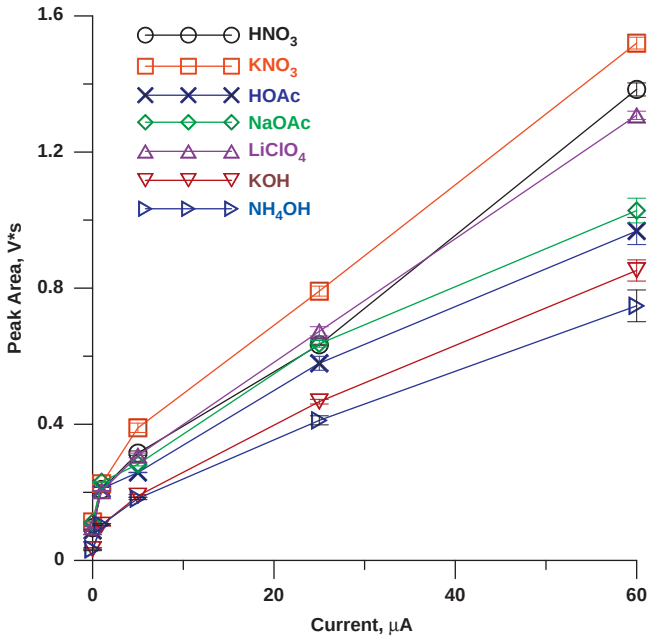

Fig. 5. Peak area as a function of applied current for analytes with varied ion mobilities. Central channel: water at 0.2 mL/min; outer channels (CEM/AEM): 1 mM HNO_3/1 mM KOH at 1.5 mL/min; sample concentration: 50 μM of each; injected volume: 26.4 μL.

on the CEM side and base (1 mM KOH) on the AEM side, etc. The signal (peak height) and S/N ratio are shown in Fig. 4 for 50 μM injected KNO_3; the noise is separately depicted in Fig. S5 in the SI. The biggest change in conductivity in changing a single electrode compartment solution occurs when water in the CEM compartment is changed to 1 mM HNO_3. However, the corresponding changes in any of the performance parameters were very minor. In contrast, reminiscent of BIMs where overall behavior (and occurrence of EFID) is much more sensitive to the AEM environment [34], changing the AEM solution to 1 mM KOH significantly reduced the voltage drop across the device, also significantly reducing the signal. But it resulted in an even greater than proportionate reduction in noise (Fig. S5), resulting in the best S/N in the a/b mode and next best in the w/b mode (Fig. 4).

3.5. *Analyte response. Effect of ion mobilities and affinities for ion exchange sites*

The behavior of fully ionized analytes was previously examined in Section 3.2 (Fig. 2) to investigate whether charge or conductivity is being detected. Here we examined a broader variety of both modestly weak and strong electrolytes, including salts, acids, and bases with a/b fluid composition and extended the study to higher i_{app} values. The analyte ions varied in their mobilities as well as affinities for the respective IEMs.

Fig. 5 shows the peak areas (note that peak heights are shown in Fig. 2) elicited by the various injected analytes (1.32 neq) as a function of i_{app}. The corresponding height based data are shown in Fig. S6. The absolute differences in peak area response among the different analytes increase with increasing i_{app}. Generally, the behaviors of these ions can be divided into three groups. First, the strong electrolytes (HNO_3, KNO_3 and $LiClO_4$), elicit the highest signal. The differences between them, although still small, are more pronounced in these area responses than in the peak height responses previously depicted in Fig. 2, suggesting that the differences are in the widths and is caused by the migration rate of the ions, whether in free solution or through the IEMs. Whereas $NaNO_3$, HNO_3 and $NaClO_4$ generate nearly equivalent peak height signals, the peak area signals for KNO_3 tend to be higher than those for HNO_3 and $LiClO_4$; the latter two generally overlap within ± 2 standard deviation bounds. Area to height ratios (a *de facto* measure of peak width; note that no chromatography is involved in these experiments) are respectively 12.6 ± 0.3, 12.4 ± 0.4 s for KNO_3 and HNO_3; there is no statistical difference between these two peak widths. The peak width for $LiClO_4$, at 13.0 ± 0.2 s is statistically different, however. The difference between KNO_3/HNO_3 and $LiClO_4$ peak widths cannot be solution mobility based as there was no difference between HNO_3 vs. KNO_3 peak widths even though H^+ has far greater mobility than K^+. Here the differences between the conductivities of $Li^+ - Na^+$ and $ClO_4^- - NO_3^-$ are substantially less. The only remaining factor is that ClO_4^- has much stronger affinity for the AEM than does NO_3^-; we reason that the slow movement of this ion through the membrane causes the greater width. The peak asymmetry values (at 5% peak height) for KNO_3, HNO_3, and $LiClO_4$ are 1.48 ± 0.12, 1.52 ± 0.12 and 1.64 ± 0.07 reflect the same pattern. The difference between KNO_3 and HNO_3 is not statistically significant to definitively ascribe asymmetry increase to the mobility difference between the cation and the anion.

A modestly weak acid HOAc and its salt NaOAc generate intermediate response. The respective peak widths are much larger at 21.5 ± 1.3 and 22.8 ± 1.2 s than the strong electrolytes. The peak asymmetries are, respectively, 1.72 ± 0.10 and 1.56 ± 0.07, suggesting that indeed greater cation–anion mobility difference contribute to greater asymmetry.

The real surprise in this series, however, comes from base injections. At all but the lowest values of i_{app}, KOH has by far the lowest response of all strong electrolytes, indeed it responds less than HOAc and has a peak width of 21.2 ± 1.2 s, comparable to that of the weak electrolytes and an asymmetry factor of 1.96 ± 0.21, substantially greater than that of HOAc. The gradual dissociation of NH_4OH makes for an even broader peak (width 29.8 ± 2.0 s) although the asymmetry remains the same (1.96 ± 0.30) as KOH. One way to account for this unusual response is an increase in the intrinsic resistance of the device when significant concentrations of OH^- ions are injected and thence brought near the AEM. If EFID of

water at the AEM contributes to lowering the dynamic resistance of the device under baseline conditions, and EFID is inhibited by the presence of OH^-, the device resistance will not drop as much on analyte injection and the observed response will be lower. This is consistent with Simons model of EFID at an AEM [22], although having tertiary amine functional groups at the AEM is crucial to his paradigm. During preparation of the synthetic AEMs, it is quite likely that some tertiary amine groups are not quaternized; it is also possible that in an alkaline environment under anodic conditions some of the quaternary ammonium functionalities degrade to tertiary amines [36,37]. It is also possible that an increase in OH^- from the central channel coming into the AEM simply increases its conductivity, thus lowering the field across it and thence decreasing EFID. In any case, fundamentally asymmetric behavior at the two ends of a pH scale are not common; this constitutes one such rare example.

The fractions of the analytes removed by the ChD_i as determined by conductivity detectors placed before and after the ChD_i are shown in Fig. S7 in the SI as a function of i_{app}. The data at very low currents are omitted as ion exchange processes occur that do not directly deal with the passage of current. These can lead to confounding results. At $i_{app}=0$, for example, for $LiClO_4$, because of greater mobility of ClO_4^- and its greater affinity for the corresponding IEM, there is more displacement of OH^- by ClO_4^-, compared to H^+ exchanged for Li^+. As a result, a net formation of LiOH (far more conductive than $LiClO_4$) occurs and conductivity actually increases: the calculation procedure returns a negative value for the fraction of $LiClO_4$ removed. With all but $LiClO_4$ and HNO_3, the removal extent remains essentially constant in the $i_{app}=5$–25 μA range. It is remarkable that KOH is nearly quantitatively removed and NH_4OH is not far behind. Note that for HOAc and NH_4OH, the fraction of conductivity remaining is not exactly equal to fraction of the analyte remaining. As conductivity increases less than linearly with concentration, the values plotted are lower limits of removal for these species.

During the review of this manuscript an anonymous reviewer pointed out that there may be potentially other explanations for the asymmetry than EFID at the AEM. One possibility is that is that the screen separating the two membranes likely contains some weakly acidic cation exchange groups. The screen may exhibit some limited ability to transport cations toward the CEM. Asymmetry may result because there is no corresponding transport mechanism for anions. This might well explain the high removal efficiency for both KOH and NH_4OH as the alkaline

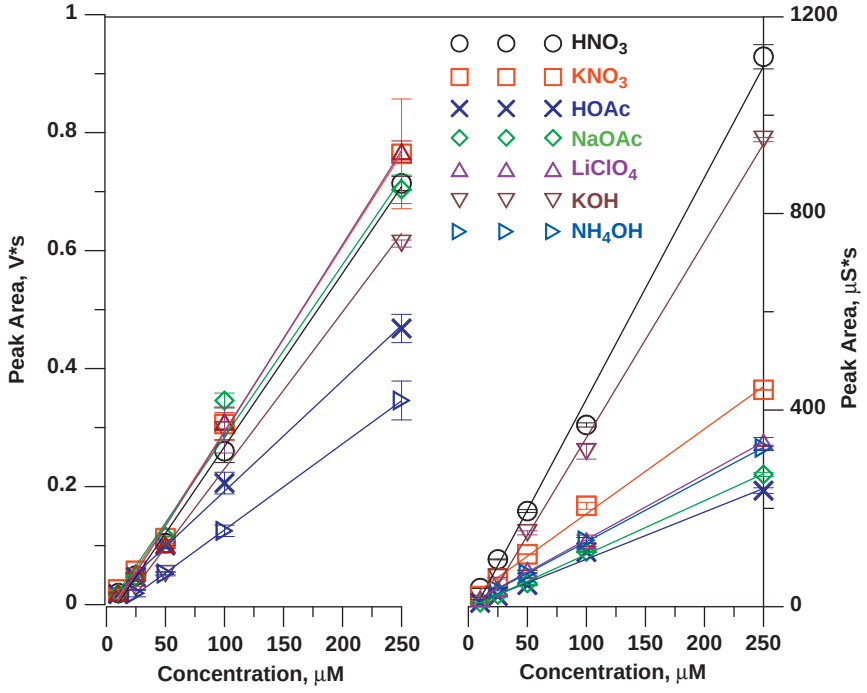

Fig. 6. Calibration curves of analytes with varied ion mobilities, obtained with ChD_i and CD, respectively. Conditions are the same as in Fig. 5. Applied current: 1 μA. Error bar indicates standard deviation ($n=3$).

Table 1
Calibration data for various analytes obtained with the ChD_i and the CD in the flow-injection mode. Conditions as in Fig. 6.

Analytes	Range (μM)	ChD_i	CD
HNO_3	10–250	$y=(2.94\pm0.07)\times10^{-3}\,x-(2.64\pm0.92)\times10^{-2}$; $r^2=0.9981$	$y=(4.52\pm0.18)x-(29.4\pm22.4)$; $r^2=0.9951$
KNO_3	10–250	$y=(3.14\pm0.09)\times10^{-3}\,x-(1.99\pm1.12)\times10^{-2}$; $r^2=0.9975$	$y=(1.73\pm0.06)x+(16.4\pm7.94)$; $r^2=0.9958$
HOAc	10–250	$y=(1.87\pm0.05)\times10^{-3}\,x+(4.71\pm6.09)\times10^{-3}$; $r^2=0.9979$	$y=(0.96\pm0.05)x+(0.73\pm5.96)$; $r^2=0.9924$
NaOAc	10–250	$y=(2.92\pm0.21)\times10^{-3}\,x-(7.61\pm25.8)\times10^{-3}$; $r^2=0.9848$	$y=(1.09\pm0.02)x-(2.88\pm2.53)$; $r^2=0.9989$
$LiClO_4$	10–250	$y=(3.18\pm0.12)\times10^{-3}\,x-(2.63\pm1.41)\times10^{-2}$; $r^2=0.9961$	$y=(1.32\pm0.01)x+(4.44\pm1.59)$; $r^2=0.9997$
KOH	25–250	$y=(2.66\pm0.33)\times10^{-3}\,x-(3.54\pm4.55)\times10^{-2}$; $r^2=0.9700$	$y=(3.98\pm0.14)x-(54.2\pm18.8)$; $r^2=0.9976$
NH_4OH	25–250	$y=(1.46\pm0.01)\times10^{-3}\,x-(1.93\pm0.16)\times10^{-2}$; $r^2=0.9999$	$y=(1.28\pm0.01)x+(4.18\pm1.90)$; $r^2=0.9998$

y denotes peak area (unit: V s for ChD_i and μS s for CD); x denotes concentration.

samples will enhance the ionization and thus the transport of cationic solutes on the surface of the "neutral" screen. We note, however, in an identical experiment with suppressed cation chromatography using a charge detector with a similar neutral screen operated in the constant voltage mode, the signals for strong base cations were not abnormally low, as in the present instance [38].

The second possibility involves the role of unavoidable contamination of CO_2 that will render the AEM, otherwise in the hydroxide form, being at least partially converted to the carbonate form. Carbonate selectivity relative to monovalent species is concentration and pH dependent and this could be at least partially responsible for the asymmetry; there is no counterpart of this for the CEM. At the present time there is insufficient evidence to conclude which one(s) of these potential possibilities play the dominant role.

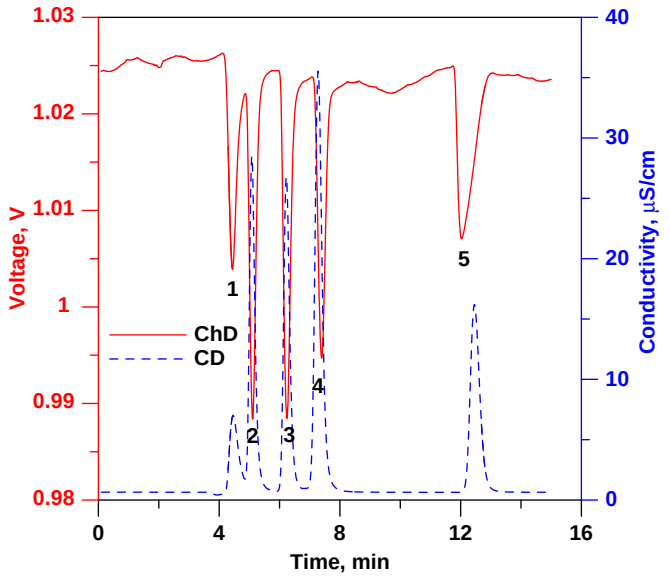

Fig. 7. Chromatograms by ChD_i and CD. i_{app}=25 μA (outer channels (CEM/AEM): 1 mM HNO_3/1 mM KOH at 1.5 mL/min). Eluent: 26 mM electrogenerated KOH at 1 mL/min; IonPac AG 16 (2 mm × 50 mm)/AS 16 (2 mm × 250 mm); ASRS Ultra-II 2-mm suppressor (all from Dionex). Injected analytes: 1, 0.1 mM acetate, 2, 0.1 mM chloride, 3, 0.1 mM nitrate, 4, 0.05 mM sulfate, 5, 0.1 mM iodide; injected volume: 26.4 μL.

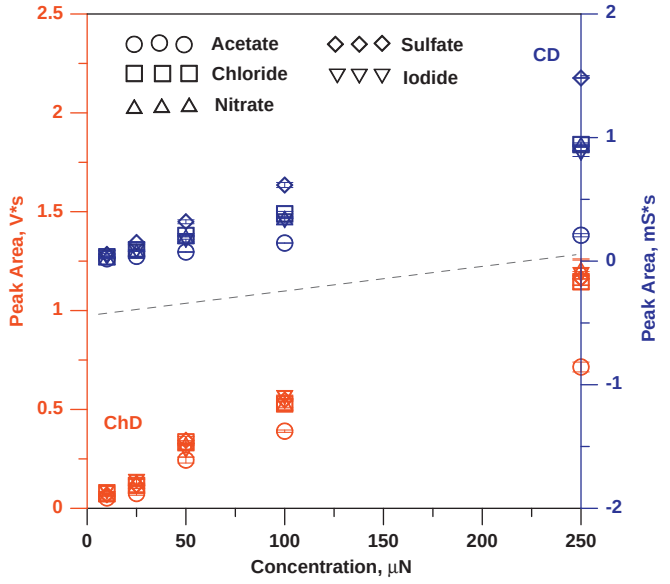

Fig. 8. Calibration curves of analytes obtained with ChD_i and CD in a chromatographic run. Conditions are the same as in Fig. 7. Error bar indicates standard deviation (n=3).

3.6. Analyte response. Calibration behavior

Fig. 6 shows the calibration curves of the same analytes obtained by a CD and a ChD_i following it. At i_{app}=1 μA, the ChD_i produces linear response behavior for the analytes over the 10–250 μM concentration range. Note that the order of response is different at the low value of i_{app} used here compared to the full current range data in Fig. 5. Except for KOH, NH_4OH and HOAc, the slopes of these plots are nearly the same, in marked contrast to the CD calibration plots. The calibration equations and uncertainties appear in Table 1; note that ChD_i calibration intercepts are much closer to zero than the CD calibration intercepts.

3.7. Use as a chromatographic detector

The ChD_i was placed after a conductivity detector (CD) in a conventional suppressed IC system. Note that in a suppressed anion chromatography system, all the analytes are converted into corresponding acids prior to entering the detectors. The chromatograms from both detectors are shown in Fig. 7. The calibration curves of the four equivalent strong electrolytes chloride, nitrate, sulfate and iodide show statistically identical slope, despite the difference in their equivalent ionic conductivities (Fig. 8), which is reflected in differences in the CD calibration slopes. The numerical calibration data obtained with both the ChD_i and the CD are shown in Table 2. The linear r^2 values are better for the CD, but the slopes are more equivalent for the ChD_i.

4. Conclusion

The ChD_i provides different and complementary information compared to the ChD operated in the constant voltage mode. Acids and bases behave asymmetrically; the unusual behavior of injected bases in this system affirms that EFID occurs primarily at the AEM and that it is inhibited by the presence of OH^-. Width and asymmetry of peaks are analyte dependent and this may have applications for analyte identification or confirmation thereof.

Table 2
Calibration data for six anions obtained with a ChD_i and a CD separated chromatographically; conditions as in Fig. 7.

Analytes	Range (μM)	ChD_i	CD
Acetate	10–250	$y=(2.74\pm0.30)\times10^{-3}\,x+(5.66\pm3.71)\times10^{-2}$; r^2=0.9649	$y=(7.77\pm1.39)\times10^{-4}\,x+(3.01\pm1.71)\times10^{-2}$; r^2=0.9124
Chloride	10–250	$y=(4.45\pm0.26)\times10^{-3}\,x+(5.29\pm3.24)\times10^{-2}$; r^2=0.9896	$y=(3.77\pm0.55)\times10^{-3}\,x+(4.38\pm6.78)\times10^{-3}$; r^2=0.9994
Nitrate	10–250	$y=(4.70\pm0.18)\times10^{-3}\,x+(4.51\pm2.20)\times10^{-2}$; r^2=0.9957	$y=(3.81\pm0.08)\times10^{-3}\,x-(1.06\pm1.01)\times10^{-2}$; r^2=0.9986
Sulfate	10–250	$y=(4.52\pm0.29)\times10^{-3}\,x+(5.44\pm3.60)\times10^{-2}$; r^2=0.9876	$y=(5.92\pm0.07)\times10^{-3}\,x+(9.50\pm9.47)\times10^{-3}$; r^2=0.9995
Iodide	10–250	$y=(4.60\pm0.19)\times10^{-3}\,x+(5.06\pm2.29)\times10^{-2}$; r^2=0.9951	$y=(3.51\pm0.05)\times10^{-3}\,x-(1.02\pm0.59)\times10^{-2}$; r^2=0.9994

y denotes peak area (unit: V s for ChD_i and μS s for CD); x denotes concentration.

Acknowledgment

We are grateful to ThermoFisher/Dionex for partially supporting this work.

Appendix A. Supporting information

Supplementary data associated with this article can be found in the online version at http://dx.doi.org/10.1016/j.talanta.2012.07.058.

References

[1] N. Maslov, Yu.A. Zolotov, Russ. Chem. Rev. 37 (1968) 310–315.
[2] B. Van Zeghbroeck, Principles of Semiconductor Devices (2011), http://ecee.colorado.edu/~bart/book/.
[3] T. Teorell, Prog. Biophys. Biophys. Chem. 3 (1953) 305–386.
[4] B. Lovreček, A. Despić, J.O.M. Bockris, J. Phys. Chem. 63 (1959) 750–751.
[5] V.J. Frilette, J. Phys. Chem. 60 (1956) 435–439.
[6] M. Senō, T. Yamabe, Bull. Chem. Soc. Jpn. 37 (1964) 668–671.
[7] K. Nagasubramanian, F.P. Chlanda, K.J. Liu, J. Membr. Sci. 2 (1977) 109–124.
[8] K.N. Mani, F.P. Chlanda, C.H. Byzewski, Desalination 68 (1988) 149–166.
[9] F.F. Kuppinger, W. Neubrand, H.J. Rapp, G. Eigenberger, Chem. Eng. Technol. 67 (1995) 731–739.
[10] J. Millman, Microelectronics, McGraw-Hill, 1979, pp. 45–48.
[11] P. Ramírez, H.J. Rapp, S. Mafé, B. Bauer, J. Electroanal. Chem. 375 (1994) 101–108.
[12] H. Holdik, A. Alcaraz, P. Ramírez, S. Mafé, J. Electroanal. Chem. 442 (1998) 13–18.
[13] S. Mafé, P. Ramírez, A. Alcaraz, Chem. Phys. Lett. 294 (1998) 406–412.
[14] R. Simons, Electrochim. Acta 29 (1984) 151–158.
[15] R. Simons, Electrochim. Acta 30 (1985) 275–282.
[16] P. Ramírez, V.M. Aquilella, J.A. Manzanares, S. Mafé, J. Membr. Sci. 73 (1992) 191–201.
[17] A. Tanioka, K. Shimizu, T. Hosono, R. Eto, T. Osaki, Colloid Surf. A 159 (1999) 395–404.
[18] M. Wien, Phys. Z. 32 (1931) 545–553.
[19] J. Schiele, Ann. Phys. 5 (1932) 811–829.
[20] J. Schiele, Phys. Z. 34 (1933) 60–64.
[21] L. Onsager, J. Chem. Phys. 2 (1934) 599–615.
[22] R. Simons, Nature 280 (1979) 824–826.
[23] H.C. Eckstrom, C. Schmelzer, Chem. Rev. 24 (1939) 367–414.
[24] J.A. Gledhill, A. Patterson Jr., J. Phys. Chem. 56 (1952) 999–1005.
[25] F.E. Bailey Jr., A. Patterson Jr., J. Am. Chem. Soc. 74 (1952) 4756–4759.
[26] B. Yang, M. Takeuchi, P.K. Dasgupta, Anal. Chem. 80 (2008) 40–47.
[27] B. Yang, F. Zhang, X. Liang, P.K. Dasgupta, J. Chromatogr. A 1216 (2009) 2412–2416.
[28] B.C. Yang, Y.J. Chen, M. Mori, S.I. Ohira, A.K. Azad, P.K. Dasgupta, K. Srinivasan, Anal. Chem. 82 (2010) 951–958.
[29] H. Small, T.S. Stevens, W.S. Bauman, Anal. Chem. 47 (1975) 1801–1809.
[30] K. Srinivasan, Abstract 230-5, Pittcon 2012, Orlando FL, March 12, 2012.
[31] T.W. Richards, W.N. Stull., Z. Phys. Chem. 42 (1903) 621.
[32] G.G. Grower, Am. Soc. Test. Mater. Proc. 17 (II) (1917) 129.
[33] Y. Chen, M. Mori, A.C. Pastusek, K.A. Schug, P.K. Dasgupta, Anal. Chem. 83 (2011) 1015–1021.
[34] Y. Tanaka, J. Membr. Sci. 303 (2007) 234–243.
[35] G. Waton, P. Mallo, S.J. Candau, J. Phys. Chem. 88 (1984) 3301–3305.
[36] A.A. Zagorodni, D.L. Kotova, V.F. Selemenev, React. Funct. Polym. 53 (2002) 157–171.
[37] V. Neagu, I. Bunia, I. Plesca, Polym. Degrad. Stab. 70 (2000) 463–468.
[38] Dr. Kannan Srinivasan, Personal Communication. ThermoFisher Dionex, 2012.